

Transient Electromagnetic Scattering of a Metallic Object Buried in Underwater Sediments

Lin-Ping Song, *Member, IEEE*, S. D. Billings, L. R. Pasion, and Douglas W. Oldenburg

Abstract—In this paper, we study the electromagnetic scattering of a conducting and permeable sphere buried in sea sediments. Instead of taking a uniform conducting medium in the previous work, we model marine environments as a layered medium that consists of the air, the sea, and the sediment. We adopt an integral equation technique to compute time-harmonic solutions for background and scattered fields under fundamental source excitations, i.e., vertical and horizontal magnetic dipoles. The corresponding transient scattering responses to causal step waveform are computed through the digital sine transform. The derived fundamental solutions provide convenient formulas tailored for three-layer medium modeling. The numerical experiments demonstrate that the scattered responses computed in the different backgrounds are approaching almost to the same decays at late times. However, the background fields can significantly mask the scattered responses. Subtracting assumed uniform background responses from “measured” total fields in the three-layered medium cannot provide a correct scattering response in the interested time range, i.e., 0.1–25 ms. To remove the background fields, we propose a conceptual gradiometer system that has receiver cubes installed radially symmetric with respect to a transmitting antenna. The results demonstrate that the suitable differential combinations are able to yield the scattering responses that well agree with those of a free space as the layered background fields in these combined receivers are equal and their influence are automatically canceled out.

Index Terms—Conducting and permeable sphere, electromagnetic induction (EMI), magnetic dipole polarization, underwater, unexploded ordnance (UXO).

I. INTRODUCTION

WIDESPREAD underwater munitions have been a big concern for increased human recreational and industrial activities and the offshore environments. The presence of water makes it difficult to detect and remove these hazardous legacies induced from wars, military training, and deliberate disposal [1]. Efforts have been put forward in investigating and developing techniques pertaining to the cleanup of underwater unexploded ordnance (UXO), including the use of acoustic waves,

Manuscript received April 12, 2015; revised August 17, 2015; accepted August 20, 2015. Date of publication September 22, 2015; date of current version January 19, 2016. This work was supported by the Strategic Environmental Research and Development Program under Grant MR-2412.

L.-P. Song and D. W. Oldenburg are with the Department of Earth, Ocean and Atmospheric Sciences, The University of British Columbia, Vancouver, BC V6T 1Z4, Canada (e-mail: lpsong@eos.ubc.ca).

S. D. Billings and L. R. Pasion are with Black Tusk Geophysics Inc., Vancouver, BC V6J 4S5, Canada.

Color versions of one or more of the figures in this paper are available online at <http://ieeexplore.ieee.org>.

Digital Object Identifier 10.1109/TGRS.2015.2473851

magnetometry, and electromagnetic induction (EMI) [2]–[6]. The latter has been successfully applied in the remediation of the land UXO [7]–[10].

In terrestrial setting, the measured magnetic fields from a subsurface metallic object in the low-frequency EMI regime are essentially magnetostatics and can be modeled in the free-space background as conduction background currents can be ignored in a typical UXO contaminated soil environment (conductivity around ~ 0.01 S/m) [11]. In contrast, marine environments are generally more conductive where an average conductivity value of seawater is around 4–5 S/m. For a survey in a conductive medium, the EMI response of a compact metallic target can be affected and might deviate from its in-air response. Norton *et al.* [4] studied the EMI response to conducting anomalies of spheroidal shape embedded in a weakly conducting host medium. Shubitidze *et al.* [5], [6] recently have used the method of auxiliary sources [11], [12] to study the scattered responses of a metallic object placed in a uniform conductive medium. Their results showed the coupling effects between the metallic objects and the conductive surrounding at early times (or at high frequencies) and that the scattered responses at late times are close to those in a free space.

However, the conductivity of ocean sediments is different from that of the sea. Depending upon porosity, sea sediments may have a conductivity value that is generally less than 1.0 S/m [14]. Given the presence of the sea–sediment conductive interface, we speculate that a simple uniform conductive space [4]–[6] may not be sufficiently good to model EMI responses of a buried object when measurements are taken close to the seafloor. In addition, there is little understanding about how the background responses in a conducting medium might mask the scattered responses of a target of interest.

The purpose of this paper is to further characterize the transient scattering responses from a buried object below the sediment. We simulate an underwater environment as a three-layered medium that consists of the air, the sea, and the sediment. For a layered electrical structure, we adopt an integral equation technique [24]–[28] to compute triaxial background and scattered fields through fundamental magnetic sources and receivers [vertical magnetic dipole (VMD) and horizontal magnetic dipole (HMD)].

The remaining part of this paper is organized as follows. Section II describes the configuration and the problem we are going to deal with. Sections III and IV present the modeling technique we adopted to compute the fields in a layered medium. The numerical results are reported in Section V. The conclusion remarks are given in Section VI.

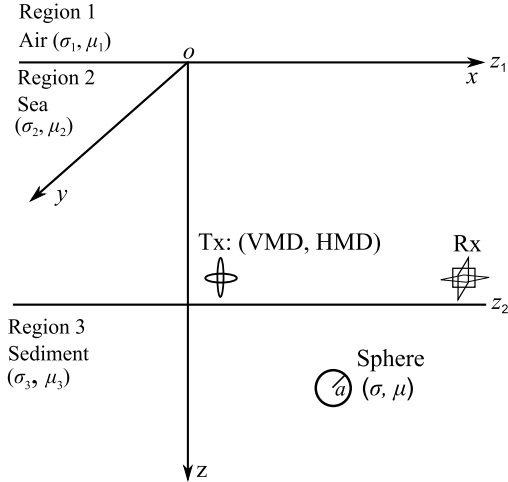


Fig. 1. Geometric configuration of the problem.

II. CONFIGURATION AND STATEMENT OF THE PROBLEM

The geometry of the problem is depicted in Fig. 1, where the positive z -axis is downward in the right-handed coordinate system. A three-layer structure, representing an underwater environment, consists of the upper half-space (region 1, air), the middle layer (region 2, seawater), and the lower half-space (region 3, sediment ground). Correspondingly, the air–sea interface is denoted at z_1 , and the sea–sediment interface is denoted at z_2 . The thickness of the middle layer or the seawater depth is given as $d = z_2 - z_1$. For convenience, we choose the origin of the z -axis at the ocean surface, i.e., $z_1 = 0$.

Assume that each layer is horizontally infinite and homogeneous. Under the quasi-static approximation of low frequencies [28], we assume that displacement currents are negligible and will not consider dielectric effects in the computation. Then, the electromagnetic (EM) properties of all three regions might be characterized by conductivity and permeability denoted as (σ_i, μ_i) , $i = 1, 2, 3$. $\mu_i = \mu_0 \mu_{ri}$, where μ_{ri} is the associated relative permeability constant and $\mu_0 = 4\pi \times 10^{-7}$ (in henries/meter). For the underwater case, the magnetic permeability of each layer is set to that of the free space. An EMI survey, where transmitter and receiver loops reside in the sea, can be taken to interrogate a metallic target buried in underwater sediments.

In this paper, we consider a small transmitting loop that is used to generate exciting fields in the three-layer medium and can be represented as a magnetic current dipole with strength m [24], [25], [28]

$$m = \frac{i\omega\mu IdS}{4\pi} \quad (1)$$

where I is the current carrying in the loop of area dS . The angular frequency is ω , and the magnetic permeability of the surrounding space is μ and $i = \sqrt{-1}$. The loop might be oriented vertically and horizontally. Therefore, we use the VMD and HMD sources to produce primary or incident fields. Similarly, we assume that three orthogonal small receiving loops, being represented as magnetic dipole receivers, are used to measure voltage responses. In this paper, the time-harmonic dependence $e^{i\omega t}$ is assumed and suppressed.

According to the EM scattering theory [28]–[30], the measured responses in the seawater are given by

$$\mathbf{d}(t) = \mathbf{d}_{\text{inc}}(t) + \mathbf{d}_{\text{sca}}(t) \quad (2)$$

where the total responses $\mathbf{d}^T = [d_x \ d_y \ d_z]$ are the sum of the associated incident fields $\mathbf{d}_{\text{inc}}(t)$ in the conducting layered structure and the scattered fields $\mathbf{d}_{\text{sca}}(t)$ due to a buried target upon excitation. To compute $\mathbf{d}_{\text{inc}}(t)$ and $\mathbf{d}_{\text{sca}}(t)$, we proceed with the integration equation technique in layered media that is formulated in the wavenumber and frequency domains [24]–[30]. Then, the corresponding transient responses are obtained through the digital Hankel transform [31].

III. FIELDS IN A THREE-LAYERED MEDIUM

The expressions for the EM fields in a half-space or an N -layered medium under the quasi-static approximation have been presented in a number of places [24]–[26], [28]. However, these expressions are either limited to a source on or above the surface or a particular source excitation like an electric dipole in a multilayered medium by Wannamaker *et al.* [26]. In addition, the variations of the formulas across the different authors make it hard to simply adopt them for our problem. In this section, we follow the potential-based derivation method [28] to briefly describe the field expressions of our interest for two types of fundamental magnetic sources (VMD and HMD) buried in a three-layered medium.

Consider the presence of magnetic sources only. The magnetic fields \mathbf{H} we are concerned can be expressed in terms of an electric vector potential \mathbf{F} [28], [29]

$$j\omega\mu\mathbf{H} = k^2\mathbf{F} + \nabla(\nabla \cdot \mathbf{F}) \quad (3)$$

where ∇ is a vectorial differential operator $(\partial/\partial x)\hat{x} + (\partial/\partial y)\hat{y} + (\partial/\partial z)\hat{z}$, and \hat{x} , \hat{y} , and \hat{z} denote the three unit coordinate vectors. In (3), k^2 is the wavenumber of a medium and defined as

$$k^2 = -i\omega\mu\sigma. \quad (4)$$

The purely imaginary squared wavenumber shows that fields of interest here are diffusive. $\nabla(\nabla \cdot \mathbf{F})$ may be explicitly expressed as

$$\nabla(\nabla \cdot \mathbf{F}) = \begin{bmatrix} \frac{\partial^2 F_x}{\partial x^2} + \frac{\partial^2 F_y}{\partial x \partial y} + \frac{\partial^2 F_z}{\partial x \partial z} \\ \frac{\partial^2 F_x}{\partial x \partial y} + \frac{\partial^2 F_y}{\partial y^2} + \frac{\partial^2 F_z}{\partial y \partial z} \\ \frac{\partial^2 F_x}{\partial x \partial z} + \frac{\partial^2 F_y}{\partial y \partial z} + \frac{\partial^2 F_z}{\partial z^2} \end{bmatrix}. \quad (5)$$

The vectorial potential satisfies the inhomogeneous Helmholtz equation [28], [29]

$$\nabla^2 \mathbf{F} + k^2 \mathbf{F} = -\mathbf{M} \quad (6)$$

where \mathbf{M} represents a magnetic source. Hence, finding \mathbf{H} fields for an arbitrary source reduces down to solving governing equation (6) for the vector potential field \mathbf{F} . Consider that the source term might be represented as $\mathbf{M}(\mathbf{r}) = \psi m \delta(\mathbf{r} - \mathbf{r}')$, where δ is the Dirac delta function and $\mathbf{r}' = (x', y', z')$ and $\mathbf{r} = (x, y, z)$ are the source and field points, respectively. Such a source expression describes a magnetic current dipole excitation with

the strength m , oriented in a unit vector $\hat{\psi}$. $\hat{\psi}$ might point in the unit coordinate direction of \hat{z} or \hat{x} or \hat{y} that corresponds to the VMD or HMD sources. Referring to Fig. 1, we present the integral representations of the potential fields that are used to compute three fundamental EM fields in a layered medium: 1) the incident fields when the source and receiver reside in the sea; 2) the incident fields that penetrate from the source in the sea down into the sediment; and 3) Green's tensor transmitting a source in the ground upward into a receiver in the sea.

A. VMD

Consider a z -directed unit magnetic dipole. In view of the symmetry of the EM properties in the problem, the fields in any of the regions can be obtained from an electric vector potential that has only a longitudinal component F_z . Namely, the vectorial potential for a VMD excitation is given as [24], [28], i.e.,

$$\mathbf{F} = F_z \hat{z}.$$

The primary potential field of the VMD is given by [24], [28], [29]

$$\mathbf{F} = m \frac{e^{-jk|\mathbf{r}-\mathbf{r}'|}}{|\mathbf{r}-\mathbf{r}'|} \hat{z}. \quad (7)$$

Equation (7) is a spherical wave function and known as the potential Green's function in an unbounded homogeneous medium. It can be expanded in terms of a cylindrical wave function as [24], [28], [30]

$$F_z = m \int_0^\infty \frac{\lambda}{\gamma} e^{-\gamma|z-z'|} J_0(\lambda\rho) d\lambda \quad (8)$$

where $\rho = \sqrt{(x-x')^2 + (y-y')^2}$, $\gamma = (\lambda^2 - k^2)^{1/2}$, λ is a radial wavenumber, and $J_0(\lambda\rho)$ is the Bessel functions of the first kind of order 0. This is the well-known Sommerfeld integral. Equation (8) is a spectral-domain representation of the fields that is a superposition of the plane waves propagating in the z -direction, modulated by the oscillatory function at a given distance between the source and field points. Following the observations in an unbounded medium, we can postulate the fields in a layered medium in a similar form to (8) by taking into account the downward and upward plane waves from the upper and lower boundaries of the layers, modifying only the z variation. In the source region, the total fields are written as the sum of the primary and secondary upward/downward fields. Then, the field amplitudes at the planar interface between two layers, for example, j and $j-1$, can be determined by imposing the EM boundary conditions for the VMD excitation. Continuity of the tangential field components of \mathbf{E} and \mathbf{H} at the interface [29], [30] leads to the boundary conditions about the potential F [24], [28]

$$\begin{aligned} F_{z,j-1} &= F_{z,j} \\ \frac{1}{\mu_{j-1}} \frac{dF_{z,j-1}}{dz} &= \frac{1}{\mu_j} \frac{dF_{z,j}}{dz}. \end{aligned} \quad (9)$$

Referring to Fig. 1, we consider the two cases: 1) VMD source in region 2; and 2) VMD source in region 3.

1) *Source in Region 2:* For the VMD in the seawater, we can write the spectral representation of fields in each layer as

$$\begin{aligned} F_{1z}(\rho, z) &= m \int_0^\infty B_1 e^{\gamma_1(z-z_1)} J_0(\lambda\rho) d\lambda, \quad z < z_1 \\ F_{2z}(\rho, z) &= m \int_0^\infty \left[A_2 e^{-\gamma_2(z-z_1)} + B_2 e^{\gamma_2(z-z_2)} \right. \\ &\quad \left. + \frac{\lambda}{\gamma_2} e^{-\gamma_2|z-z'|} \right] J_0(\lambda\rho) d\lambda, \quad z_1 < z < z_2 \\ F_{3z}(\rho, z) &= m \int_0^\infty A_3 e^{-\gamma_3(z-z_2)} J_0(\lambda\rho) d\lambda, \quad z > z_2 \end{aligned} \quad (10)$$

where F_{jz} and A_j and B_j denote the z -component potential field and the downward and upward amplitudes in layer j , respectively. Subscript 1, 2, or 3 is added to these quantities when they refer specifically to the upper half-space, the sea, and the bottom, respectively. The exponential factors in the representation might be interpreted as upward and downward waves since their decaying characteristics and approaching zero at $z = \pm\infty$. In layer 2, A_2 and B_2 are the coefficients for the downward and upward propagation waves from the air-ocean and seafloor interfaces, in addition to a direct wave term $e^{-\gamma_2|z-z'|}$. This direct term can be important for a UXO survey where a transmitter and a receiver are generally close. When observation is close to the seafloor, the upward propagation wave term $e^{\gamma_2(z-z_2)}$ can play an important role. Similarly, if observation is near the ocean surface, the downward propagation wave term $e^{-\gamma_2(z-z_1)}$ would be dominant. In layers 1 and 3, B_1 and A_3 are corresponding with the upward and downward propagation waves in the air and sediment layers. There can be no wave coming from $z = \mp\infty$; therefore, $A_1 = B_3 = 0$.

Applying the boundary conditions in (9) and after some algebraic process, we obtain

$$\begin{aligned} A_2 &= \frac{R_{21} (e^{-\gamma_2 z'} + R_{23} e^{-\gamma_2(2z_2-z')})}{1 - R_{21} R_{23} e^{-2\gamma_2 z_2}} \frac{\lambda}{\gamma_2} \\ B_2 &= \frac{R_{23} (e^{-\gamma_2(z_2-z')} + R_{21} e^{-\gamma_2(z_2+z')})}{1 - R_{21} R_{23} e^{-2\gamma_2 z_2}} \frac{\lambda}{\gamma_2} \\ A_3 &= T_{23} \frac{R_{21} e^{-\gamma_2(z_2+z')} + e^{-\gamma_2(z_2-z')}}{1 - R_{21} R_{23} e^{-2\gamma_2 z_2}} \frac{\lambda}{\gamma_2} \\ B_1 &= T_{21} \frac{R_{23} e^{-\gamma_2(2z_2-z')} + e^{-\gamma_2 z'}}{1 - R_{21} R_{23} e^{-2\gamma_2 z_2}} \frac{\lambda}{\gamma_2} \end{aligned} \quad (11)$$

where

$$\begin{aligned} R_{21} &= \frac{\mu_1 \gamma_2 - \mu_2 \gamma_1}{\mu_1 \gamma_2 + \mu_2 \gamma_1} & R_{23} &= \frac{\mu_3 \gamma_2 - \mu_2 \gamma_3}{\mu_2 \gamma_3 + \mu_3 \gamma_2} \\ T_{21} &= \frac{2\mu_1 \gamma_2}{\mu_1 \gamma_2 + \mu_2 \gamma_1} & T_{23} &= \frac{2\mu_3 \gamma_2}{\mu_2 \gamma_3 + \mu_3 \gamma_2}. \end{aligned} \quad (12)$$

Since the potential F_z produces the transverse electric (TE) fields to z , R_{21} and R_{23} may be called the TE reflection coefficients at the ocean surface and the bottom, and T_{21} and T_{23} are the TE transmission coefficients from the source in the sea into the air and the bottom.

All the four amplitude coefficients in (11) contain a common denominator $(1 - R_{21}R_{23}e^{-2\gamma_2 z_2})^{-1}$ that can be expanded as

$$\frac{1}{1 - R_{21}R_{23}e^{-2\gamma_2 z_2}} = \sum_{l=0}^{\infty} (R_{21}R_{23})^l e^{-2l\gamma_2 z_2} \quad (13)$$

if $|R_{21}R_{23}| < 1$. The condition is satisfied as long as at least one of the bounding media has even a small amount of attenuation associated with it. Equation (13) can be interpreted as the effect of multiple upward and downward traveling fields within the sea [30].

2) *Source in Region 3*: Following the same rules and notation in the above we can write the corresponding spectral representation of fields when a VMD in the sea sediment, i.e.,

$$\begin{aligned} F_{1z}(\rho, z) &= m \int_0^{\infty} B_1 e^{\gamma_1(z-z_1)} J_0(\lambda\rho) d\lambda \\ & \quad z < z_1 \\ F_{2z}(\rho, z) &= m \int_0^{\infty} \left(A_2 e^{-\gamma_2(z-z_1)} + B_2 e^{\gamma_2(z-z_2)} \right) J_0(\lambda\rho) d\lambda \\ & \quad z_1 < z < z_2 \\ F_{3z}(\rho, z) &= m \int_0^{\infty} \left(A_3 e^{-\gamma_3(z-z_2)} + \frac{\lambda}{\gamma_3} e^{-\gamma_3|z-z'|} \right) J_0(\lambda\rho) d\lambda \\ & \quad z > z_2 \end{aligned} \quad (14)$$

and the amplitudes are given as

$$\begin{aligned} A_2 &= T_{32} \frac{R_{21} e^{-\gamma_2 z_2} e^{\gamma_3(z_2-z')} \lambda}{1 - R_{21}R_{23}e^{-2\gamma_2 z_2} \gamma_3} \\ B_2 &= T_{32} \frac{e^{\gamma_3(z_2-z')} \lambda}{1 - R_{21}R_{23}e^{-2\gamma_2 z_2} \gamma_3} \\ A_3 &= \frac{(R_{21} e^{-\gamma_2 z_2} - R_{23}) e^{\gamma_3(z_2-z')} \lambda}{1 - R_{21}R_{23}e^{-2\gamma_2 z_2} \gamma_3} \\ B_1 &= T_{21} T_{32} \frac{e^{-\gamma_2 z_2} e^{\gamma_3(z_2-z')} \lambda}{1 - R_{21}R_{23}e^{-2\gamma_2 z_2} \gamma_3} \end{aligned} \quad (15)$$

where

$$T_{32} = \frac{2\mu_2\gamma_3}{\mu_2\gamma_3 + \mu_3\gamma_2}$$

is the transmission coefficient from the source in the bottom into the sea. For the field in the air, B_1 contains the product of two transmission coefficients across the seafloor and then the ocean surface. All the amplitudes undergo multiple reflections indicated by $(1 - R_{21}R_{23}e^{-2\gamma_2 z_2})^{-1}$.

B. HMD

For a horizontally directed magnetic dipole, for example, pointing in the x -direction, it induces not only a component of the potential along the dipole direction F_x but also a F_z component. The derivation process of fields is similar to the above VMD cases. The expressions for an HMD excitation are more involved than a VMD case. In addition, we have four more downward and upward amplitudes related to an HMD to be determined due to EM inhomogeneities. For the sake of clarity in presentation, we leave the HMD-related expressions in the Appendix.

The complete integral representations were derived for the potentials in the three layers. The field components in any layer can be obtained through (3). All above improper integrals like (10) and (14) are evaluated through the Anderson's digital filtering techniques [31]. Since the filtering technique was designed to have narrow band-limited filter response over a logarithmically transformed abscissa range, the numerical integration with larger values of λ is adaptively contained in the algorithm.

C. Magnetic Fields in a Uniform Space

Assume a magnetic dipole source oriented in a unit direction $\hat{\psi}$ in a uniform space. Then, the potential field at the distance r from the source is in the form of (7), with $\hat{\psi}$ replacing \hat{z} . Bringing (7) into (3), we can express the \mathbf{H} field as [37]

$$\mathbf{H} = \frac{e^{-ikr}}{4\pi r} \left\{ \left(k^2 - \frac{1}{r^2} - \frac{ik}{r} \right) \hat{\psi} - \left(k^2 - \frac{3}{r^2} - \frac{3ik}{r} \right) \mathbf{n}(\mathbf{n} \cdot \hat{\psi}) \right\} \quad (16)$$

where \mathbf{n} is a unit vector pointing from the source to the field point. For a uniform medium, the magnetic field can have components parallel and perpendicular to the unit vector \mathbf{n} . When $\hat{\psi}$ takes a unit coordinate vector, we will have the field either due to the VMD or the HMD.

IV. SCATTERING FIELD FROM A BURIED OBJECT

Following the terrestrial case, we also consider an underwater UXO survey where the dimension of a target of interest is small relative to the target-sensor distance; the primary fields around the target can be approximately uniform. Furthermore, for sufficiently low frequencies, it is possible to represent the transient scattering of a metallic object by an equivalent induced dipole. This concept has been successfully used in the interpretation of land-based EMI sensing of metallic object [15], [17], [22], [38]–[40]. Norton *et al.* [4] noted that the scattered field from a spheroid immersed in a uniform conducting medium appears dipole-like if the target size is small compared with the target range. That is, we use an induced magnetic dipole to model the so-called eddy-current response due to currents generated in the target. For a conducting medium, the perturbation of electric field due to a body in principle would produce additional EMI response that is called current channeling response (CCR). This might be modeled by an electric dipole. According to the study in [4], one main condition that

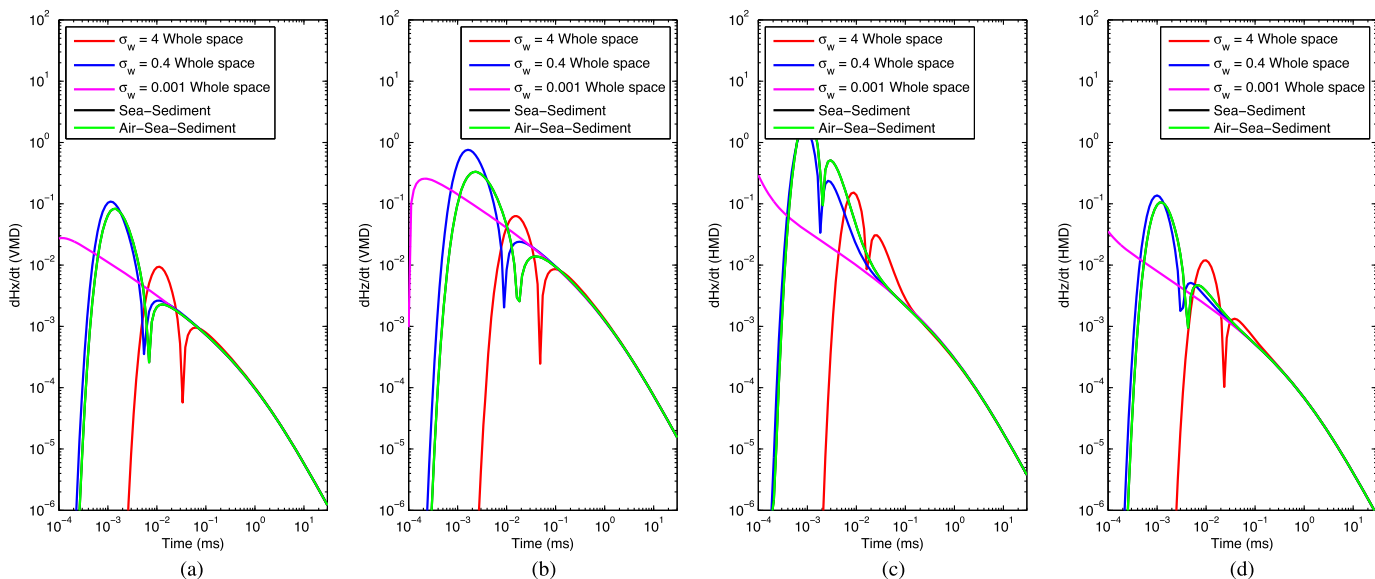


Fig. 2. Scattered responses of a dipolar sphere in different backgrounds. VMD excitation: (a) dH_x/dt . (b) dH_z/dt . HMD excitation: (c) dH_x/dt . (d) dH_z/dt .

the CCR might be significant is when the sensor–target distance is larger than the skin depth in a host medium or equivalently when measurements are concerned with the earlier times. Given that the earliest time interested in the UXO survey is about 0.1 ms and with the frequency of 10 kHz and the conductivity of 0.4 S/m of sea sediment, we estimate a minimum skin depth of 8 m. This is sufficiently greater than the deepest possible detection distance 2–3 m in the underwater. Bearing in mind these survey parameters, we anticipate that the CCR or electric dipole contribution to the EMI response is negligible in our case and thus ignore it in the formulation.

Introducing a 3×3 symmetric magnetic polarizability tensor $\mathbf{M}_s(\omega)$ that characterizes the scattering property of an object and using the Green's function method, we might express the scattered field $\mathbf{d}_{sca}(\mathbf{r}_{Rx}, \omega)$ at \mathbf{r}_{Rx} as

$$\mathbf{d}_{sca}(\mathbf{r}_{Rx}, \omega) = \mathbf{G}(\mathbf{r}_{Rx}, \mathbf{r}, \omega) \mathbf{M}_s(\omega) \mathbf{H}(\mathbf{r}, \mathbf{r}_{Tx}, \omega) \quad (17)$$

where the product $\mathbf{M}_s(\omega) \mathbf{H}(\mathbf{r}, \mathbf{r}_{Tx}, \omega)$ is the induced dipole moment [15], [19], [21], [38]–[40] in a target by the illuminating field $\mathbf{H}(\mathbf{r}, \mathbf{r}_{Tx}, \omega)$ from a transmitting antenna at \mathbf{r}_{Tx} . $\mathbf{G}(\mathbf{r}_{Rx}, \mathbf{r}, \omega)$ is the Green tensor in the background relating the field at \mathbf{r}_{Rx} due to the target at \mathbf{r} radiating into the sea. The primary \mathbf{H} and Green's tensor fields \mathbf{G} are calculated using the three-layered formulas presented in Section III for vertical and horizontal dipoles. Equation (17) is a simplified form of a full volume integral equation [26]–[28], [30], [32], [33] where we replace the total fields internal to a body by a product of a magnetic polarization tensor \mathbf{M} and a primary excitation field \mathbf{H} at a point target.

For the above approximation to be used in an underwater setting, we neglect the possible interactions between a buried object and the seafloor, assuming that the object is not close to the interface. This makes (17) easily implemented to compute the scattering of an object when its magnetic polarizabilities are known. For a general case, one might resort to solving a full-domain integral equation [26]–[28], [30], [32], [33], which

can be challenging for a very high-conductivity and permeable contrast case.

For a highly conducting and permeable object, its conductivity and relative permeability can be six to seven and two to three orders of magnitude larger than those of its surrounding medium such as sea–sediment we consider. Therefore, it might be reasonable to assume a relatively weakly conducting non-magnetic background in the simulation. With this assumption, here we use a sphere as our interest of an object for the analytic form of its magnetic polarizability under the quasi-static regime (i.e., displacement current is ignored) [34]–[36]. Given a sphere with a radius of a , relative permeability μ_r , $\mu = \mu_0 \mu_r$, and conductivity σ , the polarizability tensor might be expressed as

$$\mathbf{M}_s = -2\pi a^3 (M + iN) \mathbf{I} \quad (18)$$

where \mathbf{I} is a 3×3 identity matrix and the complex response function is given by

$$M + iN = -\frac{2\mu_r(\tanh \alpha - \alpha) + (\tanh \alpha - \alpha + \alpha^2 \tanh \alpha)}{\mu_r(\tanh \alpha - \alpha) - (\tanh \alpha - \alpha + \alpha^2 \tanh \alpha)} \quad (19)$$

and

$$\alpha = (i\omega\mu\sigma)^{\frac{1}{2}} a.$$

Having obtained the steady-state solutions to the background and secondary responses, we now proceed with the computation of the associated transient scattering responses. In the time-domain EMI sensing of UXO, the data, in general, are collected as a series of voltages after the transmitting current is shut off. The voltage measurements are related to the time derivatives of magnetic field [29]. For an idealized step-off current excitation, the time derivatives of magnetic fields are the impulse responses measured in a infinitesimal loop. Denote an EM field quantity $d(\omega)$ in the frequency domain, representing either the background fields or the secondary ones in our case. The corresponding impulse response $d(t)$ with the causality, i.e.,

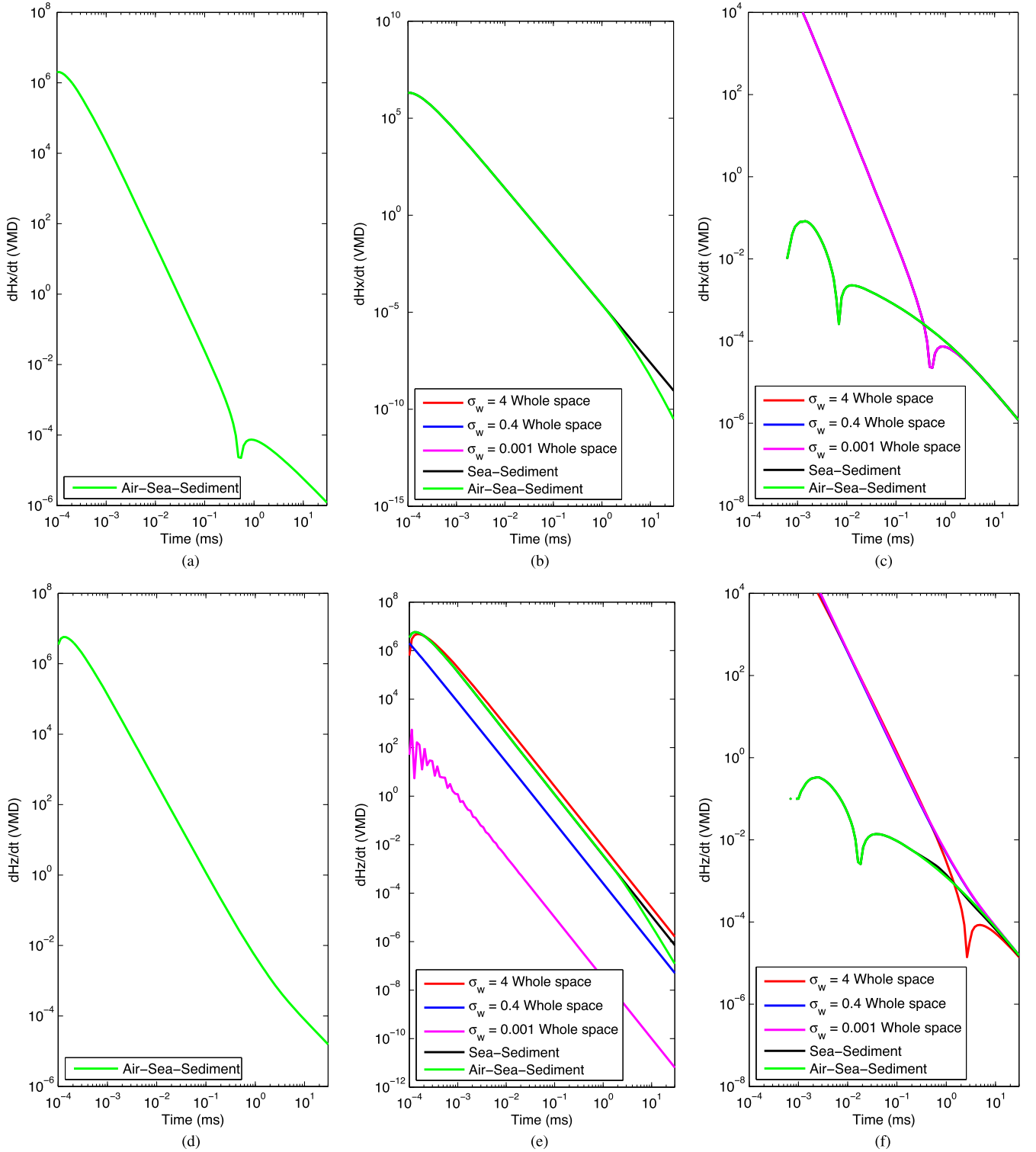


Fig. 3. Background effects on scattered responses of a dipolar sphere with VMD excitation. dH_x/dt : (a) Total. (b) Backgrounds. (c) Scattered = (a) - (b). dH_z/dt : (d) Total. (e) Backgrounds. (f) Scattered = (d) - (e).

$d(t) = 0, t < 0$, can be expressed as an inverse sine transform [27], [41]

$$d(t) = -\frac{2}{\pi} \int_0^{\infty} \text{Im}[d(\omega)] \sin \omega t \, d\omega \quad (20)$$

where $\text{Im}[\cdot]$ is an imaginary operation over a complex field. The sine transform of (20) is similarly evaluated with the digital filtering techniques [31]. For a general current excitation, the transient response can be calculated via a convolution of impulse response and transmitter waveform [23], [25].

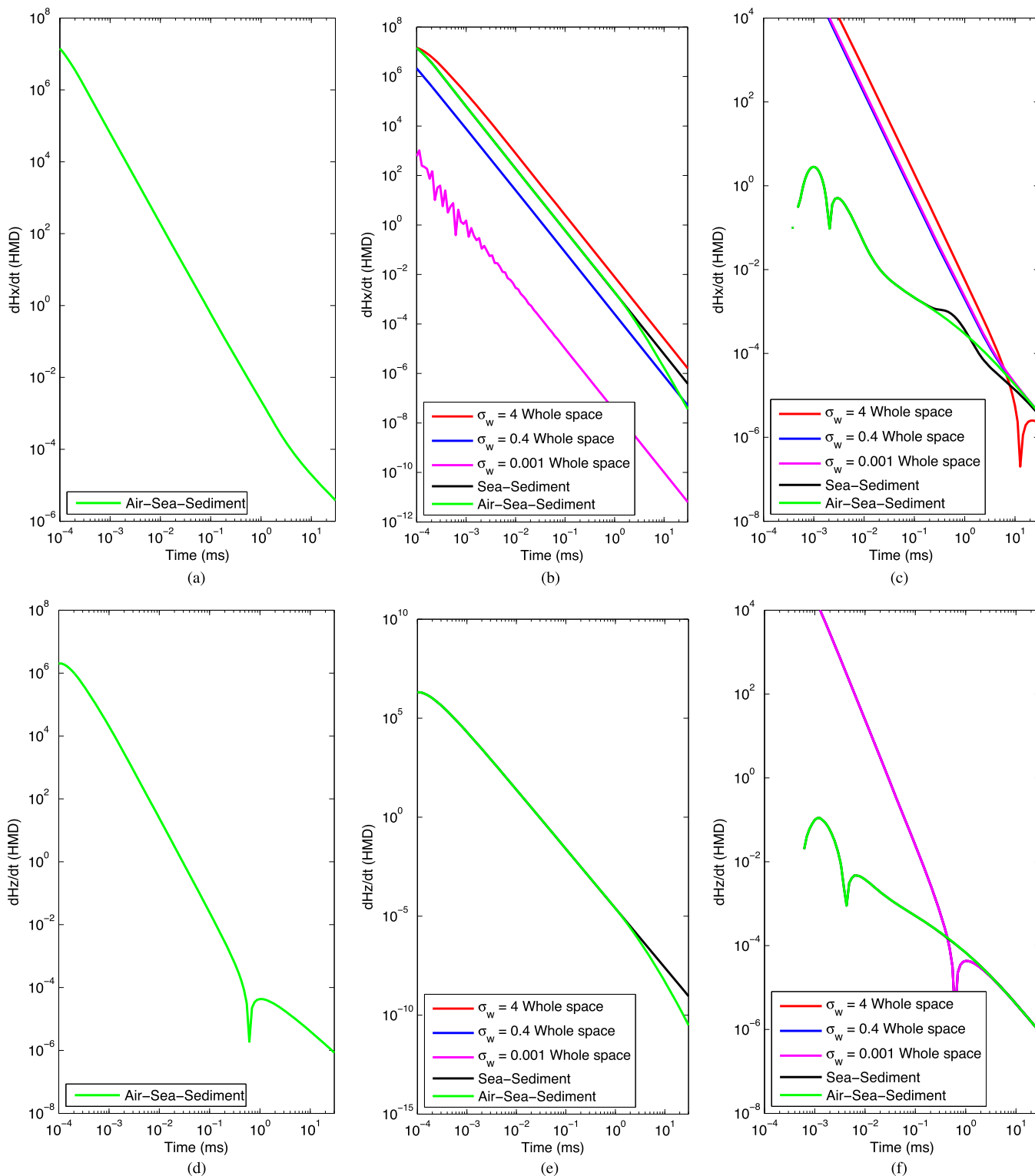


Fig. 4. Background effects on scattered responses of a dipolar sphere with HMD excitation. dH_x/dt : (a) Total. (b) Backgrounds. (c) Scattered = (a) – (b). dH_z/dt : (d) Total. (e) Backgrounds. (f) Scattered = (d) – (e).

V. EXPERIMENTS

In the following numerical studies, we model a marine environment by using the EM parameters: $\sigma_1 = 0$ S/m, $\mu_{r1} = 1$; $\sigma_2 = 4$ S/m, $\mu_{r2} = 1$; and $\sigma_3 = 0.4$ S/m, $\mu_{r3} = 1$, which represent the air, the sea, and the sediment, respectively. The air–sea and sea–sediment interfaces are at $z_1 = 0$ m and

$z_2 = 20$ m. The seawater depth $d_2 = 20$ m. A steel sphere with a radius of $a = 0.3$ m, $\sigma = 10^6$ S/m, and $\mu_r = 300$ is buried below the sediment at a depth of 3.25 m. The sphere is located at $\mathbf{r} = (0.05, 0.05, 23.25)$ m in the coordinate system. This simulates a deep object scenario in the underwater setting. Transmitters and receivers are positioned 0.1 m above the

seafloor. In the experiment, we assumed that a transmitting source is located at $\mathbf{r}_{Tx} = (0.10, -0.10, 19.9)$ m and a receiver is located at $\mathbf{r}_{Rx} = (-0.10, 0.10, 19.9)$ m. The distance between the Tx and Rx points is about 0.28 m.

We will investigate how a background can affect the scattered response from an object of interest and then consider using differential measurements for potentially removing signals due to the layered structure.

1) *Scattered Responses in Different Backgrounds:* Using the method described in Sections III and IV, we compute the scattered transient responses of the permeable and conducting sphere under the five backgrounds shown in Fig. 2. For a whole space background, we assume three conductivity values of $\sigma_w = 0.001$ S/m, $\sigma_w = 0.4$ S/m, and $\sigma_w = 4$ S/m. The true three-layer background is denoted as air–sea–sediment in the plots. The sea–sediment denoted in the plots represents the two half-space structure by ignoring the air.

For the whole space with a small conductivity value of $\sigma_w = 0.001$ S/m, the scattered response is generally decaying starting from 10^{-3} ms or earlier. With increased conductivity of $\sigma_w = 0.4$ S/m, we observe the sign reversals of the scattered responses at earlier times and shift to a bit late times around 0.1 ms for a larger conductivity value of $\sigma_w = 4$ S/m. The scattered responses of the sphere embedded in the air–sea–sediment and the sea–sediment appear to agree with each other and also exhibit the early-time sign reversals that are roughly in between the sign reversal range for both the conducting whole backgrounds. However, after about 0.1 ms, all scattered responses for the sphere buried in the five backgrounds are identically approaching to a smoothing decay. These scattering observations are consistent with the study in [5], which showed that the scattered responses of a permeable and conducting object in a uniform conducting background ($\sigma = 4$ S/m) exhibit substantial differences from those of a free space at early times.

The transient scattered responses of the embedded sphere in the free space, a uniform or layered conducting backgrounds are approaching the same decays at late times. This implies that we can assume a free-space background to compute secondary responses. However, measurements in practice are total fields as given in (2), i.e., the sum of the incident and scattered fields. To obtain scattered responses, one has to remove background or incident fields from the observed fields. Assume that, with the VMD excitation, we have the “observed” field of the x - and z -components in the sea water [see Fig. 3(a) and (d)] and have some guess of a background [see Fig. 3(b) and (e)]. By subtraction, the scattered response might be computed [see Fig. 3(c) and (f)]. In this example, the x -component of the background field in the uniform space is zero because the observation vector \mathbf{n} in (16) lies in the $x-y$ plane and is perpendicular to the direction of the VMD. Fig. 3(c) shows that, after about 3–4 ms, the x -component of the layered background signals dies out significantly, and consequently, the total field of the x -component (magenta curve) overlaps with the scattered response. For the z -component, the subtracted responses from the simple uniform backgrounds might agree with the true ones but after a much late time, for example, ~ 10 ms.

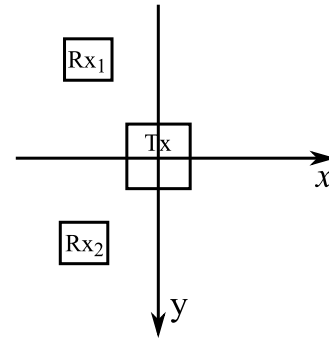


Fig. 5. Schematic of a conceptual gradiometer.

For the HMD excitation, the same subtraction experiments were conducted in Fig. 4. Referring to (16), we see that there is no z -component in a uniform background for the HMD source since $\hat{\psi} = [1 \ 0 \ 0]$ and $\mathbf{n} = [(1/\sqrt{2}) \ (1/\sqrt{2}) \ 0]$. The fields of the z -component from the HMD excitation in Fig. 4(d)–(f) are symmetrical to those of the x -component of the VMD excitation in Fig. 3(a)–(c). Overall, the subtracted responses under the HMD excitation exhibit the similar behavior to those of the VMD.

Generally, the response would shift toward low frequencies in the frequency domain when the conductivity of a background is increased [5]. Equivalently, we see that the transient responses in the uniform backgrounds shift toward late times for increasing background conductivity [see Figs. 3(e) and 4(b)]. The layered background responses are in between those of uniform media with conductivity values of 0.4–4 S/m.

The numerical experiments demonstrate that the subtraction using a uniform background model is unable to yield the correct secondary response of an object buried in the sediment and ignoring the air–sea interface can also make subtraction process inaccurate [see Figs. 3(f) and 4(c)].

2) *Differential Measurements: Removing Background Effects:* As expressed in (10) and (11), (A3) and (A4), i.e., the background EM fields either from the VMD or HMD excitations are the superposition of cylindrical wave functions that vertically propagate in the form of $e^{-\gamma z}$ and are modulated by an oscillatory Bessel function $J_0(\lambda\rho)$ or $J_1(\lambda\rho)$ at a radial distance ρ . This means that, for a given excitation, the observed background fields would be the same at two different points as long as they are at the same height and keep the same distances ρ to the source. Using this distance-dependent EM field characteristics in a layer, we can make possible subtraction of the background signals from the measurements taken in the sea. Fig. 5 shows a schematic where an excitation coil Tx is centered and two sensing coils Rx1 and Rx2 are configured in a symmetrical way to the Tx.

For this conceptual configuration, we experiment with Tx at $\mathbf{r}_{Tx} = (0.00, 0.00, 19.90)$, $\mathbf{r}_{Rx1} = (-0.10, 0.10, 19.90)$ m, and $\mathbf{r}_{Rx2} = (-0.10, -0.10, 19.90)$ m, where $\rho_1 = \rho_2 \approx 0.28$ m. The same sphere and its location in the previous experiments are used here. Fig. 6 presents the differential responses between the two receivers. In the subplots, D12XX-SCA denotes the differential measurements between the scattered

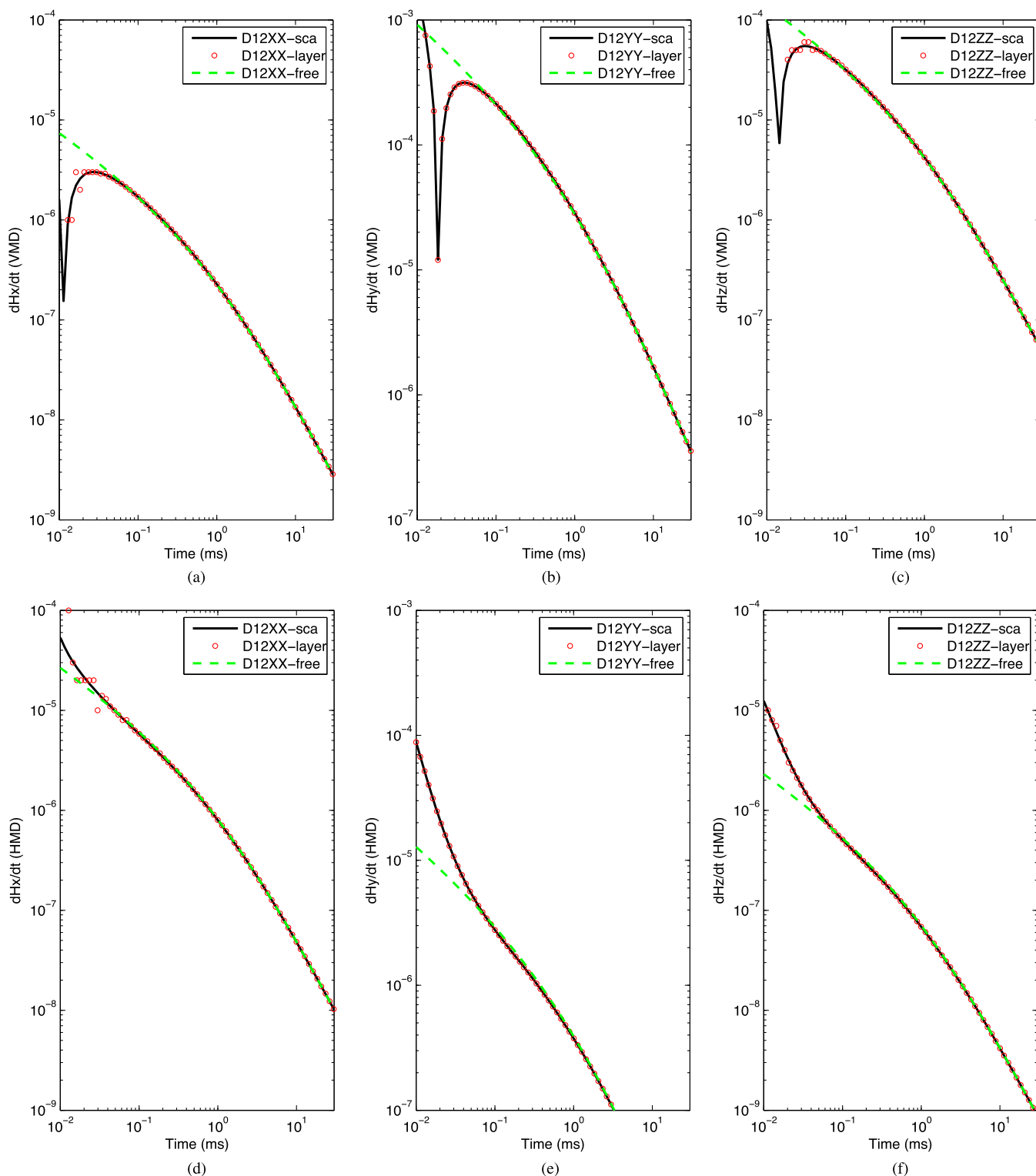


Fig. 6. Differential responses. VMD excitation: (a) x -component. (b) y -component. (c) z -component. HMD excitation: (d) x -component. (e) y -component. (f) z -component. In the subplots, `D12XX-sca` denotes the differential measurements between the scattered x -components in the three-layered medium, `D12XX-layer` denotes the total x -component in the three-layered medium, and `D12XX-free` denotes the x -component in the free space. The same notation rule applies to the y - and z -components.

x -components in the three-layered medium, `D12XX-layer` denotes the total x -component in the three-layered medium, and `D12XX-free` denotes the x -component in the free space. The same notation rule applies to the y - and z -components.

Let us see the VMD excitation case in Fig. 6(a)–(c). As expected, since the background fields in the sea can be canceled out across the two symmetrical receivers, the three differential components derived from the total fields of Rx1 and Rx2 in

the sea are equal to the differential ones from pure scattered responses at the two receivers in the sea. In addition, both differential responses taken in the sea match well with those differentials taken in the free space in the interested time range of 0.1–25 ms. The same differential results under the HMD excitation can be achieved for the three components [see Fig. 6(d)–(f)]. The experiments show that the differential measurements enable to subtract the background fields from a pair of symmetrical receivers. Therefore, in principle, their use allows us to assume that the free-space background and potentially can make underwater EMI inversion processing as simple as the land UXO case.

Hence, a sensor platform might be imagined where, for example, two receiver cubes are arranged to be radially symmetric with respect to a transmitting loops. The EM fields due to a layer structure are the same theoretically for such symmetric receiver cubes. Thus, the combination of recordings between the two cubes could provide a kind gradiometer measurement to remove the background signals. The preliminary numerical experiment demonstrated the feasibility of such a conceived differential instrument.

VI. CONCLUSION

In this paper, we have applied an integral equation technique to compute the transient scattering responses of a conducting and permeable sphere buried in sea sediments. Underwater environments are treated as a three-layer medium, which consists of the air, the sea, and the ground. In the computation, a polarizability tensor model is used to analytically represent the EMI characteristics of a metallic sphere under assumption of a large sensor–target distance. We observed that, at early times, the scattered responses of the buried sphere in uniform and layered conducting backgrounds all exhibit some sign reversals and are substantially different from each other. After certain late time, for example, around 0.1 ms, the scattered responses computed in the different backgrounds are approaching toward the same decays. These scattering phenomena are consistent with the previous study [5]. However, inspecting the total fields that are actually recorded, we found that a background field can significantly mask the scattered responses. The experiments show that subtracting assumed uniform background responses from “measured” total fields in the three-layered medium cannot provide a correct scattering response in the interested time range of 0.1–25 ms. Considering that a layered background field is the cylindrical wave superposition, we conjecture a system that has receiver cubes installed radially symmetric with respect to a transmitting antenna. As these receivers have the same background fields in magnitude, background fields can be removed by combing the responses measured at the receivers. The results demonstrate that the differential measurements yield the scattering responses that well agree with those of free space as the influences of the layered background fields are automatically canceled out. Further work will focus on verification using experimental data with an extension of the integral technique to a finite-size loop.

APPENDIX

FIELDS IN A THREE-LAYERED MEDIUM DUE TO HMD

Consider a horizontally directed magnetic dipole, for example, pointing in the x -direction. Due to the electrical inhomogeneity along the z -direction, the horizontal excitation not only induces a component of the potential along the dipole direction F_x but also a z component. Therefore, \mathbf{F} takes the form as [24], [28]

$$\mathbf{F} = F_x \hat{x} + F_z \hat{z}. \quad (\text{A1})$$

Applying continuity of the tangential field components of \mathbf{E} and \mathbf{H} at the interface leads to the boundary conditions about the potential F for the x -oriented HMD [24], [28]

$$\begin{aligned} F_{z,j-1} &= F_{z,j} \\ \frac{1}{\mu_{j-1}} \left(\frac{dF_{x,j-1}}{dx} + \frac{dF_{z,j-1}}{dz} \right) &= \frac{1}{\mu_j} \left(\frac{dF_{x,j}}{dx} + \frac{dF_{z,j}}{dz} \right) \\ \sigma_{j-1} F_{x,j-1} &= \sigma_j F_{x,j} \\ \frac{dF_{x,j-1}}{dz} &= \frac{dF_{x,j}}{dz}. \end{aligned} \quad (\text{A2})$$

Same as the VMD cases, we also present the spectral representations of the potential fields in the two cases:

3) *Source in Region 2*: When the dipole source is in region 2, the potential fields in the three regions are given

$$\begin{aligned} F_{1x} &= \int_0^\infty B_1 e^{\gamma_1(z-z_1)} J_0(\lambda\rho) d\lambda \\ F_{1z} &= -\frac{x}{\rho} \int_0^\infty D_1 e^{\gamma_1(z-z_1)} \lambda J_1(\lambda\rho) d\lambda \\ F_{2x} &= \int_0^\infty \left[A_2 e^{-\gamma_2(z-z_1)} + B_2 e^{\gamma_2(z-z_2)} \right. \\ &\quad \left. + \frac{\lambda}{\gamma_2} e^{-r_2|z-z'|} \right] J_0(\lambda\rho) d\lambda \\ F_{2z} &= -\frac{x}{\rho} \int_0^\infty \left(C_2 e^{-\gamma_2(z-z_1)} + D_2 e^{\gamma_2(z-z_2)} \right) \lambda J_1(\lambda\rho) d\lambda \\ F_{3x} &= \int_0^\infty A_3 e^{-\gamma_3(z-z_2)} J_0(\lambda\rho) d\lambda \\ F_{3z} &= -\frac{x}{\rho} \int_0^\infty C_3 e^{-\gamma_1(z-z_2)} \lambda J_1(\lambda\rho) d\lambda. \end{aligned} \quad (\text{A3})$$

Because of induced F_z components, there are a total of eight coefficients that need to be determined. A_2 , B_2 , A_3 , and B_1 are related to the primary excitation F_x ; C_2 , D_2 , C_3 , and D_1

are related to the induced excitation F_z . After some deal of algebraic manipulations, we have

$$\begin{aligned}
A_2 &= \frac{\hat{R}_{21} \left[e^{-\gamma_2 z'} + \hat{R}_{23} e^{-\gamma_2 (2z_2 - z')} \right] \lambda}{1 - \hat{R}_{21} \hat{R}_{23} e^{-2\gamma_2 z_2}} \frac{\lambda}{\gamma_2} \\
B_2 &= \frac{\hat{R}_{23} \left[e^{-\gamma_2 (z_2 - z')} + \hat{R}_{21} e^{-\gamma_2 (z_2 + z')} \right] \lambda}{1 - \hat{R}_{21} \hat{R}_{23} e^{-2\gamma_2 z_2}} \frac{\lambda}{\gamma_2} \\
A_3 &= (1 - \hat{R}_{23}) \frac{e^{-\gamma_2 (z_2 - z')} + \hat{R}_{21} e^{-\gamma_2 (z_2 + z')}}{1 - \hat{R}_{21} \hat{R}_{23} e^{-2\gamma_2 z_2}} \frac{\lambda}{\gamma_3} \\
B_1 &= (1 - \hat{R}_{21}) \frac{e^{-\gamma_2 z'} + \hat{R}_{23} e^{-\gamma_2 (2z_2 - z')}}{1 - \hat{R}_{21} \hat{R}_{23} e^{-2\gamma_2 z_2}} \frac{\lambda}{\gamma_1} \\
C_2 &= \frac{(\mu_1 \gamma_2 + \mu_2 \gamma_1)^{-1} S_1 - R_{21} (\mu_2 \gamma_3 + \mu_3 \gamma_2)^{-1} e^{-\gamma_2 z_2} S_2}{1 - R_{21} R_{23} e^{-2\gamma_2 z_2}} \\
D_2 &= -\frac{R_{23} (\mu_1 \gamma_2 + \mu_2 \gamma_1)^{-1} e^{-\gamma_2 z_2} S_1 - (\mu_2 \gamma_3 + \mu_3 \gamma_2)^{-1} S_2}{1 - R_{21} R_{23} e^{-2\gamma_2 z_2}} \\
S_1 &= \frac{2(\mu_1 \sigma_1 - \mu_2 \sigma_2)}{\sigma_1 \gamma_2 + \sigma_2 \gamma_1} \left[\frac{e^{-\gamma_2 z'} + \hat{R}_{23} e^{-\gamma_2 (2z_2 - z')}}{1 - \hat{R}_{21} \hat{R}_{23} e^{-2\gamma_2 z_2}} \right] \lambda \\
S_2 &= \frac{2(\mu_3 \sigma_3 - \mu_2 \sigma_2)}{\sigma_3 \gamma_2 + \sigma_2 \gamma_3} \left[\frac{e^{-\gamma_2 (z_2 - z')} + \hat{R}_{21} e^{-\gamma_2 (z_2 + z')}}{1 - \hat{R}_{21} \hat{R}_{23} e^{-2\gamma_2 z_2}} \right] \lambda \\
D_1 &= C_2 + e^{-\gamma_2 z_2} D_2 \\
C_3 &= C_2 e^{-\gamma_2 z_2} + D_2
\end{aligned} \tag{A4}$$

where

$$\hat{R}_{21} = \frac{\sigma_1 \gamma_2 - \sigma_2 \gamma_1}{\sigma_1 \gamma_2 + \sigma_2 \gamma_1} \quad \hat{R}_{23} = \frac{\sigma_3 \gamma_2 - \sigma_2 \gamma_3}{\sigma_2 \gamma_3 + \sigma_3 \gamma_2} \tag{A5}$$

are the reflection coefficients for the HMD from the sea surface and the sea bottom, respectively. \hat{R}_{21} and \hat{R}_{23} explicitly involve in electrical conductivity values in the two layers for HMD. In contrast, R_{21} and R_{23} in (12) explicitly involve in magnetic permeability parameters in the relevant two layers for VMD. From the secondary source terms S_1 and S_2 , we do see the that EM inhomogeneities in the layers introduce additional contribution F_z to the fields.

4) *Source in Region 3*: When the dipole source is in region 3, the potential fields in the three regions are given

$$\begin{aligned}
F_{1x} &= \int_0^\infty B_1 e^{\gamma_1 (z - z_1)} J_0(\lambda \rho) d\lambda \\
F_{1z} &= -\frac{x}{\rho} \int_0^\infty D_1 e^{\gamma_1 (z - z_1)} \lambda J_1(\lambda \rho) d\lambda \\
F_{2x} &= \int_0^\infty \left(A_2 e^{-\gamma_2 (z - z_1)} + B_2 e^{\gamma_2 (z - z_2)} \right) J_0(\lambda \rho) d\lambda \\
F_{2z} &= -\frac{x}{\rho} \int_0^\infty \left(C_2 e^{-\gamma_2 (z - z_1)} + D_2 e^{\gamma_2 (z - z_2)} \right) \lambda J_1(\lambda \rho) d\lambda \\
F_{3x} &= \int_0^\infty \left(A_3 e^{-\gamma_3 (z - z_2)} + \frac{\lambda}{\gamma_3} e^{-r_3 |z - z'|} \right) J_0(\lambda \rho) d\lambda \\
F_{3z} &= -\frac{x}{\rho} \int_0^\infty C_3 e^{-\gamma_1 (z - z_2)} \lambda J_1(\lambda \rho) d\lambda
\end{aligned} \tag{A6}$$

$$\begin{aligned}
A_2 &= \frac{(1 + \hat{R}_{23}) \hat{R}_{21} e^{-\gamma_2 z_2} e^{\gamma_3 (z_2 - z')}}{1 - \hat{R}_{21} \hat{R}_{23} e^{-2\gamma_2 z_2}} \frac{\lambda}{\gamma_2} \\
B_2 &= \frac{(1 + \hat{R}_{23}) e^{\gamma_3 (z_2 - z')}}{1 - \hat{R}_{21} \hat{R}_{23} e^{-2\gamma_2 z_2}} \frac{\lambda}{\gamma_2} \\
A_3 &= \frac{(\hat{R}_{21} e^{-2\gamma_2 z_2} - \hat{R}_{23}) e^{\gamma_3 (z_2 - z')}}{1 - \hat{R}_{21} \hat{R}_{23} e^{-2\gamma_2 z_2}} \frac{\lambda}{\gamma_3} \\
B_1 &= \frac{(1 - \hat{R}_{21})(1 + \hat{R}_{23}) e^{-\gamma_2 z_2} e^{\gamma_3 (z_2 - z')}}{1 - \hat{R}_{21} \hat{R}_{23} e^{-2\gamma_2 z_2}} \frac{\lambda}{\gamma_1} \\
C_2 &= \frac{(\mu_1 \gamma_2 + \mu_2 \gamma_1)^{-1} S_1 - R_{21} (\mu_2 \gamma_3 + \mu_3 \gamma_2)^{-1} e^{-\gamma_2 z_2} S_2}{1 - R_{21} R_{23} e^{-2\gamma_2 z_2}} \\
D_2 &= \frac{R_{23} (\mu_1 \gamma_2 + \mu_2 \gamma_1)^{-1} e^{-\gamma_2 z_2} S_1 - (\mu_2 \gamma_3 + \mu_3 \gamma_2)^{-1} S_2}{1 - R_{21} R_{23} e^{-2\gamma_2 z_2}} \\
S_1 &= \frac{2(\mu_1 \sigma_1 - \mu_2 \sigma_2)}{\sigma_1 \gamma_2 + \sigma_2 \gamma_1} \left[\frac{(1 + \hat{R}_{23}) e^{-\gamma_2 z_2} e^{\gamma_3 (z_2 - z')}}{1 - \hat{R}_{21} \hat{R}_{23} e^{-2\gamma_2 z_2}} \right] \lambda \\
S_2 &= \frac{2(\mu_3 \sigma_3 - \mu_2 \sigma_2)}{\sigma_3 \gamma_2 + \sigma_2 \gamma_3} \left[\frac{(1 + \hat{R}_{21}) e^{-2\gamma_2 z_2} e^{\gamma_3 (z_2 - z')}}{1 - \hat{R}_{21} \hat{R}_{23} e^{-2\gamma_2 z_2}} \right] \lambda \\
D_1 &= C_2 + e^{-\gamma_2 z_2} D_2 \\
C_3 &= C_2 e^{-\gamma_2 z_2} + D_2.
\end{aligned} \tag{A7}$$

Similar to the VMD excitation, (A4)–(A7) show that the multiple reflections of the HMD are with $(1 - \hat{R}_{21} \hat{R}_{23} e^{-2\gamma_2 z_2})^{-1}$ for the primary amplitudes. However, for the induced amplitudes, the multiple reflections involve in both $(1 - R_{21} R_{23} e^{-2\gamma_2 z_2})^{-1}$ and $(1 - \hat{R}_{21} \hat{R}_{23} e^{-2\gamma_2 z_2})^{-1}$ in a complicated manner.

For the y -directed HMD, \mathbf{F} is in the form

$$\mathbf{F} = F_y \hat{x} + F_z \hat{z} \tag{A8}$$

and replacing F_x with F_y leads to the same expressions as (A3)–(A7).

ACKNOWLEDGMENT

The authors would like to thank the editor and reviewers for their constructive comments that help improve the manuscript.

REFERENCES

- [1] A. Schwartz and E. Brandenburg, "An overview of underwater technologies for operations involving underwater munitions," *Marine Technol. Soc. J.*, vol. 43, no. 4, pp. 62–75, 2009.
- [2] "On acoustic detection and classification of UXO in the underwater environment," Strategic Environ. Res. Develop. Program (SERDP)/Office of Naval Res. Workshop, Alexandria, VA, USA, Sep. 2013.
- [3] S. Keenan, J. A. Young, C. P. Foley, and J. Du, "2010. A high-Tc flip-chip SQUID gradiometer for mobile underwater magnetic sensing," *Supercond. Sci. Technol.*, vol. 23, no. 2, pp. 25–29, 2010.
- [4] S. J. Norton, W. A. SanFilippo, and I. J. Won, "Eddy-current and current-channeling response to spheroidal anomalies," *IEEE Trans. Geosci. Remote Sens.*, vol. 43, no. 10, pp. 2200–2209, Oct. 2005.
- [5] F. Shubitidze, B. Barrowes, I. Shamatava, J. P. Fernández, and K. O'Neill, "Underwater UXO detection and discrimination: Understanding EMI scattering phenomena in a conducting environment," in *Proc. SPIE*, 2008, pp. 1–11.
- [6] F. Shubitidze, B. Barrowes, I. Shamatava, J. P. Fernández, and K. O'Neill, "Underwater UXO discrimination studies: Adapting EMI forward models to marine environments," in *Proc. SPIE*, Apr. 13–17, 2009, vol. 7303, pp. 1–10.

- [7] E. Gasperikova, J. T. Smith, H. F. Morrison, A. Becker, and K. Kappler, "UXO detection and identification based on intrinsic target polarizabilities," *Geophysics*, vol. 74, pp. B1–B9, 2009.
- [8] S. D. Billings *et al.*, "Unexploded ordnance discrimination using magnetic and electromagnetic sensors: Case study from a former military site," *Geophysics*, vol. 75, no. 3, pp. B103–B114, 2010.
- [9] L. Beran *et al.*, "Practical strategies for classification of unexploded ordnance," *Geophysics*, vol. 78, no. 1, pp. E41–E46, 2013.
- [10] A. Bijamov *et al.*, "Camp Butner live-site UXO classification using hierarchical clustering and Gaussian mixture modeling," *IEEE Trans. Geosci. Remote Sens.*, vol. 52, no. 8, pp. 5218–5229, Aug. 2014.
- [11] F. Shubitidze, K. O'Neill, K. Sun, I. Shamatava, and K. D. Paulsen, "A hybrid full MAS and combined MAS/TSA algorithm for electromagnetic induction problems sensing," *Appl. Comput. Electromagn. Soc. J.*, vol. 19, no. 1b, pp. 112–127, Mar. 2004.
- [12] F. Shubitidze, K. O'Neill, S. A. Haider, K. Sun, and K. D. Paulsen, "Application of the method of auxiliary sources to the wideband electromagnetic induction problem," *IEEE Trans. Geosci. Remote Sens.*, vol. 40, no. 4, pp. 928–942, Apr. 2002.
- [13] K. Sun, K. O'Neill, F. Shubitidze, I. Shamatava, and K. Paulsen, "Theoretical analyses of TSA formulation and its domain of validity," *IEEE Trans. Geosci. Remote Sens.*, vol. 42, no. 9, pp. 1871–1881, Sep. 2004.
- [14] A. D. Chave, S. Constable, and R. N. Edwards, "Electrical exploration methods in applied geophysics," in *Electrical Exploration Methods for the Seafloor*, vol. 2. Tulsa, OK, USA: SEG Books, ch. 12, 1991.
- [15] Y. Das, J. E. McFee, J. Toews, and G. C. Stuart, "Analysis of an electromagnetic induction detector for real-time localization of buried objects," *IEEE Trans. Geosci. Remote Sens.*, vol. 28, no. 3, pp. 278–287, May 1990.
- [16] A. Sebak, L. Shafai, and Y. Das, "Near-zone fields scattered by three-dimensional highly conducting permeable objects in the field of an arbitrary loop," *IEEE Trans. Geosci. Remote Sens.*, vol. 29, no. 1, pp. 9–15, Jan. 1991.
- [17] L. Carin *et al.*, "On the wideband EMI response of a rotationally symmetric permeable and conducting target," *IEEE Trans. Geosci. Remote Sens.*, vol. 39, no. 6, pp. 1206–1213, Jun. 2001.
- [18] I. J. Won, D. A. Keiswetter, and T. H. Bell, "Electromagnetic induction spectroscopy for clearing landmines," *IEEE Trans. Geosci. Remote Sens.*, vol. 39, no. 4, pp. 703–709, Apr. 2001.
- [19] L. Pasion and D. W. Oldenburg, "A discrimination algorithm for UXO using time domain electromagnetics," *J. Eng. Environ. Geophys.*, vol. 28, pp. 91–102, 2001.
- [20] Y. Zhang, L. Collins, H. Yu, C. Baum, and L. Carin, "Sensing of unexploded ordnance with magnetometer and induction: Theory and signal processing," *IEEE Trans. Geosci. Remote Sens.*, vol. 41, no. 5, pp. 1005–1015, May 2003.
- [21] J. T. Smith and H. F. Morrison, "Estimating equivalent dipole polarizabilities for the inductive response of isolated conductive bodies," *IEEE Trans. Geosci. Remote Sens.*, vol. 42, no. 6, pp. 1208–1214, Jun. 2004.
- [22] L. R. Pasion, "Inversion of time domain electromagnetic data for the detection of unexploded ordnance," Ph.D. dissertation, Univ. British Columbia, Vancouver, BC, USA, 2007.
- [23] L.-P. Song, F. Shubitidze, L. R. Pasion, D. W. Oldenburg, and S. D. Billings, "Computing transient electromagnetic responses of a metallic object using a spheroidal excitation approach," *IEEE Geosci. Remote Sens. Lett.*, vol. 5, no. 3, pp. 359–363, Jul. 2008.
- [24] J. R. Wait, *Electromagnetic Waves in Stratified Media*. New York, NY, USA: Pergamon, 1970.
- [25] J. R. Wait, *Geo-Electromagnetism*. New York, NY, USA: Academic, 1982.
- [26] P. E. Wannamaker, G. W. Hohmann, and W. A. SanFilippo, "Electromagnetic modeling of three-dimensional bodies in layered earths using integral equations," *Geophysics*, vol. 49, pp. 60–77, 1984.
- [27] G. A. Newman, G. W. Hohmann, and W. L. Anderson, 1986. "Transient electromagnetic response of a three-dimensional body in a layered earth," *Geophysics*, vol. 51, no. 8, pp. 1608–1627, Aug. 1986.
- [28] S. H. Ward and G. W. Hohmann, "Electromagnetic theory for geophysical applications," in *Electromagnetic Methods in Applied Geophysics, Volume 1—Theory*, M. N. Nabighian, Ed. Tulsa, OK, USA: Soc. Exploration Geophys., 1988, pp. 131–311.
- [29] R. F. Harrington, *Time-Harmonic Electromagnetic Fields*. New York, NY, USA: Wiley-IEEE Press, 2001.
- [30] W. C. Chew, *Waves and Fields in Inhomogeneous Media*. New York, NY, USA: Wiley-IEEE Press, ch. 2, 1999.
- [31] W. L. Anderson, "Fast Hankel transforms using related and lagged convolutions," *ACM Trans. Math. Softw.*, vol. 8, no. 4, pp. 344–368, Dec. 1982.
- [32] L.-P. Song and Q. H. Liu, "A new approximation to three-dimensional electromagnetic scattering," *IEEE Geosci. Remote Sens. Lett.*, vol. 2, no. 2, pp. 238–242, Apr. 2005.
- [33] C. G. Farquharson, K. Duckworth, and D. W. Oldenburg, "Comparison of integral equation and physical scale modelling of the electromagnetic responses of models with large conductivity contrasts," *Geophysics*, vol. 71, no. 4, pp. G169–G177, Jul/Aug. 2006.
- [34] J. R. Wait, "A conducting sphere in a time-varying magnetic field," *Geophysics*, vol. 16, no. 4, pp. 666–672, 1951.
- [35] S. H. Ward, "Unique determination of conductivity, susceptibility, size, and depth in multifrequency electromagnetic exploration," *Geophysics*, vol. 24, no. 3, pp. 531–546, 1959.
- [36] F. S. Grant and G. F. West, *Interpretation Theory in Applied Geophysics*. New York, NY, USA: McGraw-Hill, Section 6.5, 1965.
- [37] J. D. Jackson, *Classical Electrodynamics*, 2nd ed. New York, NY, USA: Wiley, 1975, pp. 180–182.
- [38] B. Barrow and H. H. Nelson, "Model-based characterization of electromagnetic induction signatures obtained with the MTADS electromagnetic array," *IEEE Trans. Geosci. Remote Sens.*, vol. 39, no. 6, pp. 1279–1285, Jun. 2001.
- [39] J. T. Miller, T. Bell, J. Soukup, and D. Keiswetter, "Simple phenomenological models for wideband frequency-domain electromagnetic induction," *IEEE Trans. Geosci. Remote Sens.*, vol. 39, no. 6, pp. 1294–1298, Jun. 2001.
- [40] T. H. Bell, B. J. Barrow, and J. T. Miller, "Subsurface discrimination using electromagnetic induction sensors," *IEEE Trans. Geosci. Remote Sens.*, vol. 39, no. 6, pp. 1286–1293, Jun. 2001.
- [41] G. B. Arfken and H. J. Weber, *Mathematical Methods for Physicists*, 4th ed. San Diego, CA, USA: Academic, 1995.
- Lin-Ping Song** (M'06), photograph and biography not available at the time of publication.
- S. D. Billings**, photograph and biography not available at the time of publication.
- L. R. Pasion**, photograph and biography not available at the time of publication.
- Douglas W. Oldenburg**, photograph and biography not available at the time of publication.